



Accurate 77-GHz Millimeter-Wave Radar Noncontact Vital Sign Detection Using the Optimized Variational Mode Decomposition Algorithm

Yuefeng Zhao¹ · Kun Wang¹ · Jing Gao²

Received: 6 November 2022 / Revised: 30 March 2023 / Accepted: 31 March 2023 / Published online: 21 June 2023
© The Author(s), under exclusive licence to Springer Science+Business Media, LLC, part of Springer Nature 2023

Abstract

Respiration and heartbeat are important vital signs of the human body. More detection systems, for these vital signs, especially for noncontact measurements, are being developed. However, owing to the large amount of noise in the signals, the accurate separation of respiratory and heartbeat signals has become challenging in the field of vital sign detection. We propose an optimized variational mode decomposition (VMD) method to realize the accurate separation of respiratory and heartbeat signals. We apply the relative entropy and sample entropy to optimize the VMD (RESE-VMD) algorithm and introduce the RESE-VMD method into 77-GHz millimeter-wave radar signal processing. The ideal parameters of the variational model are searched by relative entropy, and each modal function and central frequency are continuously updated to effectively avoid modal confounding. The signal is reconstructed by selecting the appropriate signal components according to the sample entropy and correlation coefficient. Accordingly, we build real experimental scenarios for the experiments; the results show that our method achieves better performance in separating respiratory and heartbeat signals. Our results pave the way for important applications in clinical noncontact vital sign detection.

Keywords Vital sign detection · Variational mode decomposition · Relative entropy · Sample entropy · RESE-VMD

1 Introduction

In recent years, human vital sign detection has become a topic of great interest in the field of biological signal detection. The vital sign signal detection system mainly includes two categories: contact and noncontact detection systems [1]. Contact detection systems usually use contact-based sensors to obtain the heart rate [2], which easily causes cross infection and makes detection inconvenient. Therefore, more scholars have begun to pay attention to research on noncontact detection systems. Noncontact vital sign detection methods have been extensively developed [3]. The millimeter-wave radar system is the mainstream vital sign monitoring method [4, 5]. Noncontact millimeter-wave radar system is more portable, comfortable, and noninvasive than contact detection systems. They eliminate the limitation of

contact measurements. Moreover, noncontact measurements are more suitable for individuals who are sensitive to contact measurements, including infants, burn victims, and patients with infectious diseases [6]. In [7], the authors proposed a noncontact vital sign monitoring in a bedroom. The whole analysis relies on a unique phase unwrapping process. The system effectively suppresses the effects of phase noise. As a result, millimeter-wave radar has been widely used in heart-rate detection in recent years.

Human vital signs play a key role in the field of vital sign detection. Respiration and the heartbeat are greatly important vital signals. A large number of studies have focused on the separation of respiratory and heartbeat signals. Fixed band-pass filtering does not always produce reliable findings because of interference from tiny movements and the varying frequency of vital signs in different people [8]. Several adaptive filtering approaches have been developed to filter noise in the data and properly separate respiratory and heartbeat signals, including wavelet transform (WT) [9], empirical mode decomposition (EMD) [10], complete ensemble empirical mode decomposition (CEEMD) [11], and variational mode decomposition (VMD) [12]. Yang et al. [13] proposed applying wavelet packet transform to decompose the signal

✉ Jing Gao
21128541@qq.com

¹ School of Physics and Electronics, Shandong Normal University, Jinan, China

² Library, Shandong Normal University, Jinan, China

into low-frequency and high-frequency components to form a subspace tree. WT can decompose the signal into different frequency components through multi-scale analysis. The method has good time-frequency localization characteristics. Kumar et al. [14] proposed an EMD method to eliminate electrocardiogram signal noise. Cheng et al. [15] proposed using CEEMD to remove the baseline wandering noise. Zheng et al. [16] proposed using VMD weighted reconstruction of the second harmonic of the heartbeat to estimate the heart rate. Zhang et al. [17] proposed a novel adaptive parameter optimization VMD algorithm that extracts vital signs from a signal containing residual noise. The VMD algorithm has a high level of efficacy and can overcome mode aliasing. The iterative approach and modal components in the VMD model are used to obtain the best solution. The VMD model can simultaneously deconstruct multi-component signals. In the processing of nonlinear and nonstationary signals, it is highly effective. The VMD algorithm decomposes the signal into multiple intrinsic mode functions (IMFs) and residual noise [18]. Respiratory and heartbeat signals are separated according to the center frequency and correlation coefficient. However, it is difficult to choose the correct wavelet function and decomposition layer based on the WT method. The method based on CEEMD has the problems of the endpoint effect and modal confounding [19]. Some scholars have proposed optimizing the VMD model to fulfill the segregation of vital sign signals from noise [20]. The process requires the manual determination of the optimal parameters of the model. It is prone to issues like inadequate and excessive decomposition, and it diminishes the denoising impact.

To solve the issues mentioned above, we propose an optimized VMD method to realize the accurate separation of respiratory and heartbeat signals. We apply the relative entropy and sample entropy to optimize the VMD (RESE-VMD) algorithm and introduce the RESE-VMD method to radar signal processing. The ideal parameters of the variational model are searched by relative entropy, and each modal function and central frequency are continuously updated to effectively avoid modal confounding. The signal is reconstructed by selecting the appropriate signal components according to the sample entropy and correlation coefficient. We build real experimental scenarios for experiments, and the experimental results show that our method achieves better performance in separating respiratory and heartbeat signals.

Our major contributions are as follows.

- We propose a VMD method based on relative entropy and sample entropy adaptive optimization, which achieves the separation of respiratory and heartbeat signals.
- We build real experimental scenarios to conduct multiple sets of experiments.
- The experimental results show that our method achieves better performance in separating respiratory and heartbeat signals.

The remainder of the paper is organized as follows, Section 2 introduces the theoretical introduction and parameter selection; Section 3 shows the experimental settings; Section 4, we discuss the simulation and experimental results; In Section 5, we conclude our work in this paper.

2 Materials and Methods

In this section, we will introduce the acquisition and processing of millimeter-wave radar signals. The separation and accurate extraction of the respiratory heartbeat signal is achieved using the RESE-VMD algorithm. The system algorithm flow is shown in Fig. 1.

2.1 Signal Acquisition and Processing

The electromagnetic wave signal of the radar system is reflected after being impeded in its transmission path by various objects [21]. The transmitting signal and the receiving signal enter the mixer for mixing. The difference between the transmitting signal and the receiving signal is obtained, which is the intermediate frequency (IF) signal [22, 23].

The transmitted signal of 77-GHz millimeter-wave radar based on frequency-modulated continuous wave (FMCW) radar [24] $X_{TS}(t)$ is defined as

$$X_{TS}(t) = A_{TS} \cos\left(2\pi f_s t + \pi \frac{B}{T_{dt}} t^2 + \theta(t)\right) \quad (1)$$

where f_s denotes the starting frequency, A_{TS} is the transmitted signal's amplitude, $\theta(t)$ represents the phase noise, B denotes the bandwidth, and T_{dt} represents the duration of the chirp signal pulse. Let $x(t)$ denote the displacement of the front-to-back movement of the chest and c denote the velocity of light. The time delay is $D = 2x(t)/c$. Currently, the echo signal $X_{RS}(t)$ is

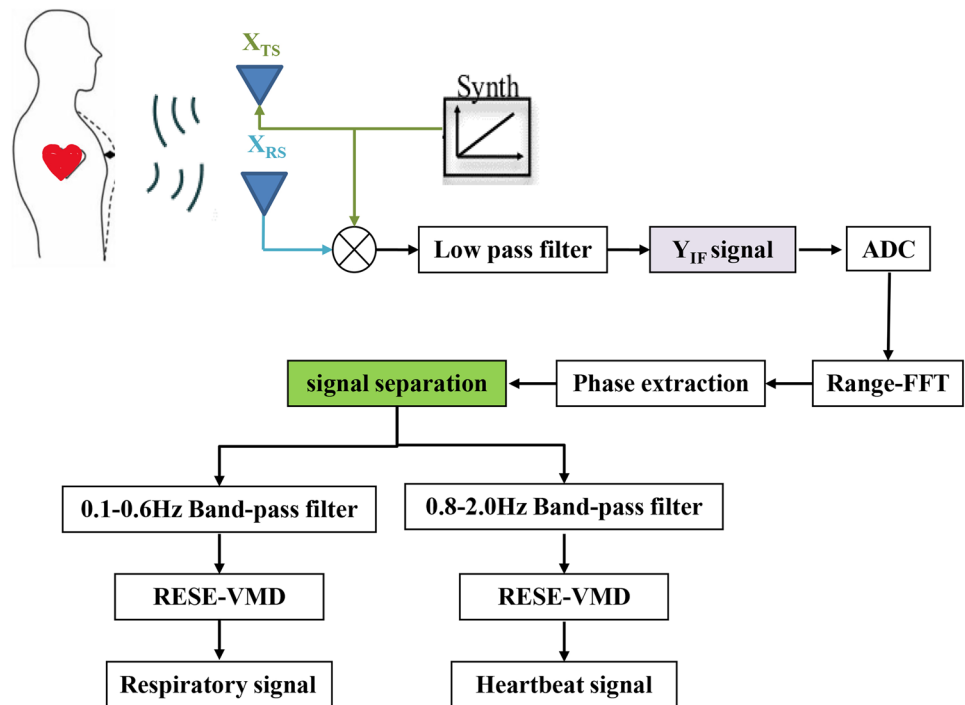
$$X_{RS}(t) = A_{RS} \cos\left(2\pi f_s(t - D) + \pi \frac{B}{T_{dt}}(t - D)^2 + \theta(t - D)\right) \quad (2)$$

which mixes the echo and transmitted signals from the two quadrature I/Q channels and filters out the interfering signals using a low-pass filter to produce the IF signal $Y_{IF}(t)$,

$$Y_{IF}(t) = A_{TS} A_{RS} \exp\left(j\left(2\pi \frac{2Bx(t)}{cT_{dt}} t + \frac{4\pi x(t)}{\lambda}\right)\right) \quad (3)$$

The transmission antenna, reception antenna, radio frequency components, analog components (e.g., clocks), and analog-to-digital converters (ADCs) make up the entire

Figure 1 System algorithm flow of noncontact vital sign detection. X_{TS} represents the millimeter-wave radar transmit signal. X_{RS} represents the millimeter-wave radar reception signal. Y_{IF} represents the intermediate frequency signal after mixing and filtering of the transmitted and received signals.



77-GHz millimeter-wave radar system. In our system, Texas Instruments’ IWR1642 millimeter-wave radar is used for signal acquisition. It has low power consumption and is harmless to humans.

In this work, the signal generator adopts the time-division multiplexing technique. First, multiple transmitting antennas transmit FMCW signals to the target. Then, the receiving antennas receive the return signal. Finally, we analyze and process the respiratory and heartbeat signals. Specifically, the transmitting antenna transmits continuous waves to the surface of the human chest cavity. The echo signal reflected by the measurement target is received by the radar receiver. The echo signal is mixed with the transmit signal by a quadrature receiver. Further, the mixed signal is passed through a filter to extract a valid signal. Next, the valid signal is sampled by an ADC and processed by MATLAB software, such as fast Fourier transform (FFT), phase extraction, and signal separation. Finally, the time domain and frequency domain information of respiration and the heartbeat are obtained. Respiration and the heartbeat are known to cause vibrations on the surface of the chest cavity, and static reflectors in the same range of the target during measurement (e.g., stationary body parts, furniture) produce direct current offsets, which can lead to nonlinear combinations of doppler signals, resulting in phase distortion. We use the moving target indication (MTI) method based on the principle of pulse cancellation to achieve static clutter removal.

2.2 Variational Mode Decomposition

A novel approach to adaptive signal processing is VMD, which aims to decompose a real-valued input signal $z(t)$ into multiple modes. The procedure is essentially the answer to the variational problem in terms of achieving effective signal separation from a low to high frequency. The constraint variational expression can be written as

$$\min_{\{\phi_k\}, \{\psi_k\}} \left\{ \sum_k \left\| \partial_t \left[\left(\delta(t) + \frac{j}{\pi t} \right) * \phi_k(t) \right] e^{-j\psi_k t} \right\|_2^2 \right\} \tag{4}$$

$$s.t. \sum_{k=1}^k \phi_K = z(t)$$

where $\{\phi_k\} = \{\phi_1, \phi_2, \dots, \phi_K\}$ and $\{\psi_k\} = \{\psi_1, \psi_2, \dots, \psi_K\}$ represent all modes of decomposition as well as their respective central frequencies. Here, $\|\cdot\|_2$ represents the L^2 -norm. The bandwidth is estimated through the squared L^2 -norm of the gradient. k stands for the number of decomposition layers. A unit pulse function is $\delta(t)$. j is a fictional unit. $*$ represents the convolution operation. The computed partial derivative is denoted by ∂_t .

In a noisy environment, the quadratic penalty factor α ensures the effectiveness of signal extraction [25], while the Lagrange multiplier λ reduces the constraint requirement [26]. The restricted variational problem represented in Eq. (4) is turned into an unconstrained variational issue, and the augmented Lagrange expression is derived as

$$L(\{\phi_k\}, \{\psi_k\}, \lambda) = \alpha \sum_k \|\partial_t \left[\left(\delta(t) + \frac{j}{\pi t} \right) * \phi_k(t) \right] e^{-j\psi_k t} \|_2^2 + \|\ z(t) - \sum_k \phi_k(t) \|_2^2 + \langle \lambda(t), z(t) - \sum_k \phi_k(t) \rangle \tag{5}$$

The augmented Lagrange is sought by iteratively updating ϕ_k^{n+1} , ψ_k^{n+1} , and λ_k^{n+1} to obtain the optimal the solution to the constrained variational model.

$$\hat{\phi}_k^{n+1}(\psi) \leftarrow \frac{\hat{z}(\psi) - \sum_{i < k} \hat{\phi}_i^{n+1}(\psi) - \sum_{i > k} \hat{\phi}_i^n(\psi) + \hat{\lambda}(\psi)/2}{1 + 2\alpha(\psi - \psi_k^n)^2} \tag{6}$$

$$\psi_k^{n+1} \leftarrow \frac{\int_0^\infty \psi |\hat{\phi}_k^{n+1}(\psi)|^2 d\psi}{\int_0^\infty |\hat{\phi}_k^{n+1}(\psi)|^2 d\psi} \tag{7}$$

$$\hat{\lambda}^{n+1}(\psi) \leftarrow \hat{\lambda}^n(\psi) + \tau \left(\hat{z}(\psi) - \sum_k \hat{\phi}_k^{n+1}(\psi) \right) \tag{8}$$

where $\hat{\lambda}$ stands for Fourier transform, n represents the number of iterations, τ means fidelity. Finally, the iteration stops when the following formula is satisfied:

$$\sum_k \frac{\|\hat{\phi}_k^{n+1} - \hat{\phi}_k^n\|_2^2}{\|\hat{\phi}_k^n\|_2^2} < V \tag{9}$$

where V denotes the tolerance of the convergence standard. The standard default value is 1×10^{-7} .

2.3 Relative Entropy and Sample Entropy

VMD is greatly affected by parameters, but an artificial setting cannot achieve the best result. k and α are the key factors that determine the quality of signal decomposition [27]. When both k and α are small, the two signals are easily mixed. When α is small and k is large, some decomposed components may contain noise. When both k and α are large, an important part of the signal may be decomposed into two or more decomposed components. When α is large and k is small, the target signal is easily lost in the noise. As a result, in order to determine the optimal parameters accurately and quickly, we use the relative entropy optimization VMD in this paper to realize the effective decomposition of the signal. According to the optimized VMD, the vital sign signal is carried out through decomposition, and we calculate the relative entropy of the intrinsic mode function. The corresponding k with the lowest relative entropy and α with the lowest relative entropy are selected.

Firstly, the range of k is set as [2–10] and the range of α is set as [100–2000]. Then, we initialize the parameters k and α after inputting the signal. It is worth noting that the k to be 2 and the α to be 100. Finally, perform a variational

modal decomposition of the signal and calculate the relative entropy minimum for each component. Based on relative entropy minimum, ours obtain the k value corresponding to it, and further find the value of α corresponding to the relative entropy minimum according to the optimal k value. The algorithm optimization flow chart is shown in Fig. 2.

Relative entropy is equivalent to the information entropy difference between the real probability distribution and theoretical probability distribution [28].

$$D(M \parallel N) = \sum_{i=1}^N \left[M(x_i) \log \frac{M(x_i)}{N(x_i)} \right] \tag{10}$$

$M(x_i)$ shows the probability distribution of the actual data, and $N(x_i)$ represents the theoretical probability distribution. When the two groups of data are more similar, the relative entropy is smaller, and vice versa. Choose k and α with the lowest relative entropy. The decomposed signal component includes the dominant signal component and the dominant noise component. In this paper, the signal component and noise component are determined by sample entropy [29, 30].

For the time series $\{x(n)\} = x(1), x(2), \dots, x(N)$ composed of N data, a set of vector sequences $X_m(1), \dots, X_m(N - m + 1)$ with dimension M is formed by a serial number.

$$X_m(i) = \{x(i), x(i + 1), \dots, x(i + m + 1)\} \tag{11}$$

$$1 \leq i \leq N - M + 1$$

Define the distance $d[X_m(i), X_m(j)]$ between vector $X_m(i)$ and $X_m(j)$ as the absolute value of the maximum difference between their corresponding elements.

$$d[X_m(i), X_m(j)] = \max_{k=0,1,\dots,m-1} (|x(i+k) - x(j+k)|) \tag{12}$$

For a given $X_m(i)$, count the number of j whose distance between $X_m(i)$ and $X_m(j)$ is less than or equal to r , and call it Z_i .

$$Z_i^m(r) = \frac{1}{N-m-1} Z_i \tag{13}$$

$$Z^{(m)}(r) = \frac{1}{N-m} \sum_{i=1}^{N-m} Z_i^m(r) \tag{14}$$

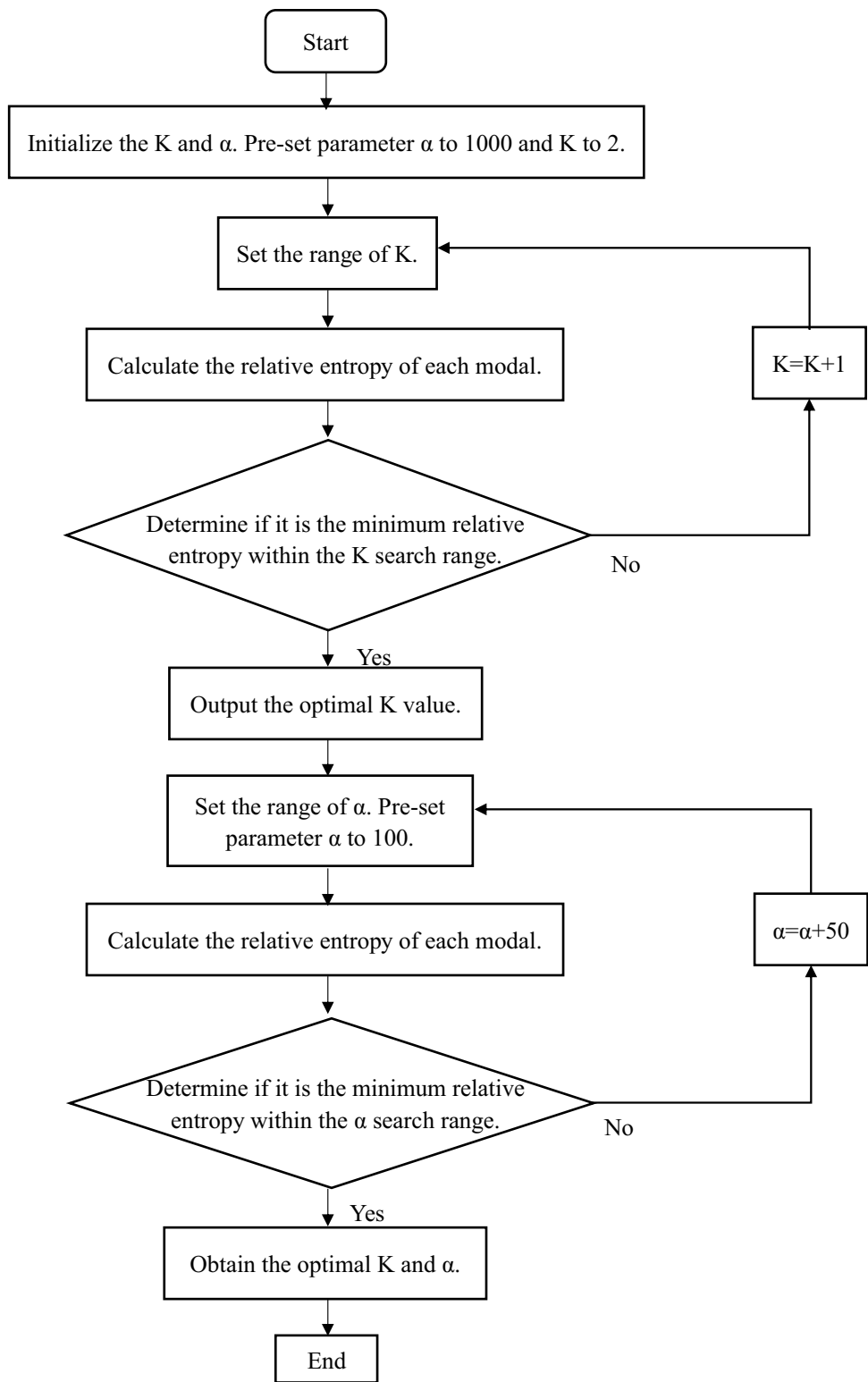
$Z^{(m)}(r)$ is the probability of two series matching m points with a similar tolerance r . Increase the dimension to $m + 1$, count the number of j whose distance between $X_{m+1}(i)$ and $X_{m+1}(j)$ is less than or equal to r , and call it A_i . A_i is defined as

$$A_i^m(r) = \frac{1}{N-m-1} A_i \tag{15}$$

$$A^{(m)}(r) = \frac{1}{N-m} \sum_{i=1}^{N-m} A_i^m(r) \tag{16}$$

$A^{(m)}(r)$ is the probability of two series matching $m + 1$ points. The sample entropy is denoted as

Figure 2 Flow chart of the optimization algorithm proposed in this paper.



$$SE(m, r) = \lim_{N \rightarrow \infty} \left\{ -\ln \left[\frac{A^{(m)}(r)}{Z^{(m)}(r)} \right] \right\}$$

when N is finite, it is defined as

$$SE(m, r, N) = -\ln \left[\frac{A^{(m)}(r)}{Z^{(m)}(r)} \right]$$

(17) **2.4 Signal Denoising and Reconstruction**

The optimal value of k and α are calculated by relative entropy. The optimized VMD method is performed to disassemble the initial signal that is divided into k intrinsic mode functions, and the sample entropy function is calculated for

(18)

each intrinsic mode function. The signal is denoised and reconstructed according to sample entropy, correlation parameters, and center frequency. The signal-to-noise ratio (SNR) before and after denoising is calculated as

$$SNR = 10 \log_{10} \frac{\sum_{k=1}^K F^2(k)}{\sum_{k=1}^K [f(k) - F(k)]^2} \quad (19)$$

where F represents the original signal, and f denotes the denoising signal.

3 Results

3.1 Experimental Scene and Parameter Setting

In this section, we analyze the performance of the noncontact vital sign detection system. The experimental scene is shown in Fig. 3, where the measured target is in a stationary position in a chair at a distance of 0.5–1 m from the radar sensor system.

The experimental parameters are shown in Table 1. Frequency Modulated Continuous Wave (FMCW) millimeter-wave radar sensors are becoming increasingly popular in several applications where system requirements and parameter selection vary. Distance requirements, distance resolution, maximum speed requirements, sensor field of view, data memory etc. are all influencing factors. Frequency slope, scanning bandwidth etc. can affect system performance. The

Table 1 Radar configuration parameters.

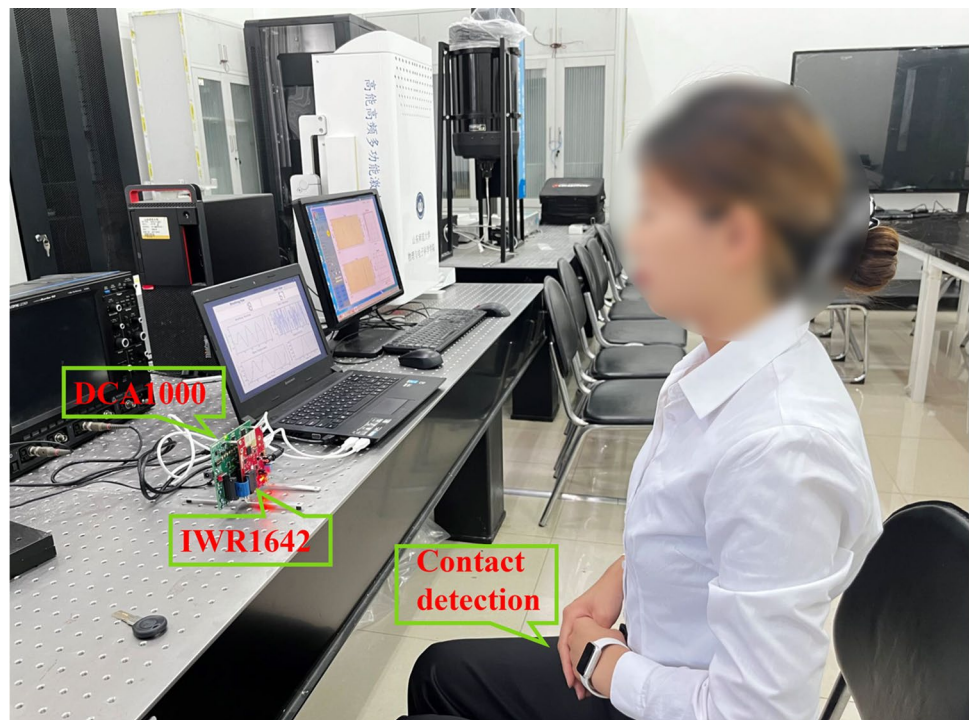
Parameter	Configuration
Start frequency (f_s)	77 GHz
Frequency slope (F_s)	70 MHz/ μ s
Frequency modulation period (T_{dt})	57 μ s
Bandwidth (B)	3.99 GHz
ADC samples (M)	256
Chirp loops	128
ADC Sampling rate (M_s)	4.49 Msps

maximum and minimum distance at which a radar sensor can detect a target is an important parameter for radar sensors. In addition, distance resolution is another important metric. The minimum distance between two objects that allows them to be detected as separate objects is known as the distance resolution. This depends primarily on the chirp scan bandwidth that the radar sensor can provide. TI's radar devices support a scan bandwidth of 4 GHz, allowing a distance resolution as low as approximately 4 cm. The formula for calculating the maximum distance is shown below

$$Range_{max} = \frac{IF_{max} * c}{2F_s} = \frac{M_s * T_{dt} * c}{2B} = M * \frac{c}{2B} \quad (20)$$

where IF_{max} represents maximum IF bandwidth supported. IF_{max} is also dependent on the ADC sampling frequency (M_s) used. c represents speed of light. F_s represents slope of the transmitted chirp. The distance resolution is calculated as

Figure 3 The schematic diagram of experiment scene. DCA1000 and IWR1642 represent ADC data acquisition board and integrated single-chip millimeter-wave sensor based on FMCW radar technology, respectively. The watch is used as the reference sensor for heart rate detection to evaluate the accuracy of the noncontact detection system.



$$Range_{resolution} = \frac{1}{M_s} \frac{F_s * T_{dt} * c}{2B} = \frac{c}{2B} \tag{21}$$

where B represents sweep bandwidth of FMCW chirp.

$$B = F_s * T_{dt} \tag{22}$$

The distance resolution of the system is calculated to be 3.76 cm. The fast time sampling of the IF signal allows for the acquisition of target distance information, while the slow time sampling allows for the acquisition of information such as target speed and respiratory heartbeat. When the ADC sampling point is 256, the maximum detection distance is 9.63 m, which meets the environmental requirements for indoor vital signs detection. Based on the number of fast time samples and the number of slow time samples the received data size can be calculated as 512 KB. The

system’s parameters are set with high distance resolution and detection accuracy. And the received data storage size is moderate.

3.2 Comparison with Other Methods in Simulation Experiments

The respiratory signal’s frequency range is 0.1–0.6 Hz, while that of the heartbeat signal is 0.8-2 Hz. When the noise frequency is within the range of respiration and the heartbeat frequency, it is easy to produce errors, especially if the heartbeat signal is weak and prone to respiratory harmonic interference. As a result, we propose that the optimized VMD method be used to deconstruct and rebuild the signal for denoising and that the relative entropy algorithm

Figure 4 Denoising results of WT, CEEMD, and RESE-VMD on the respiratory signal.

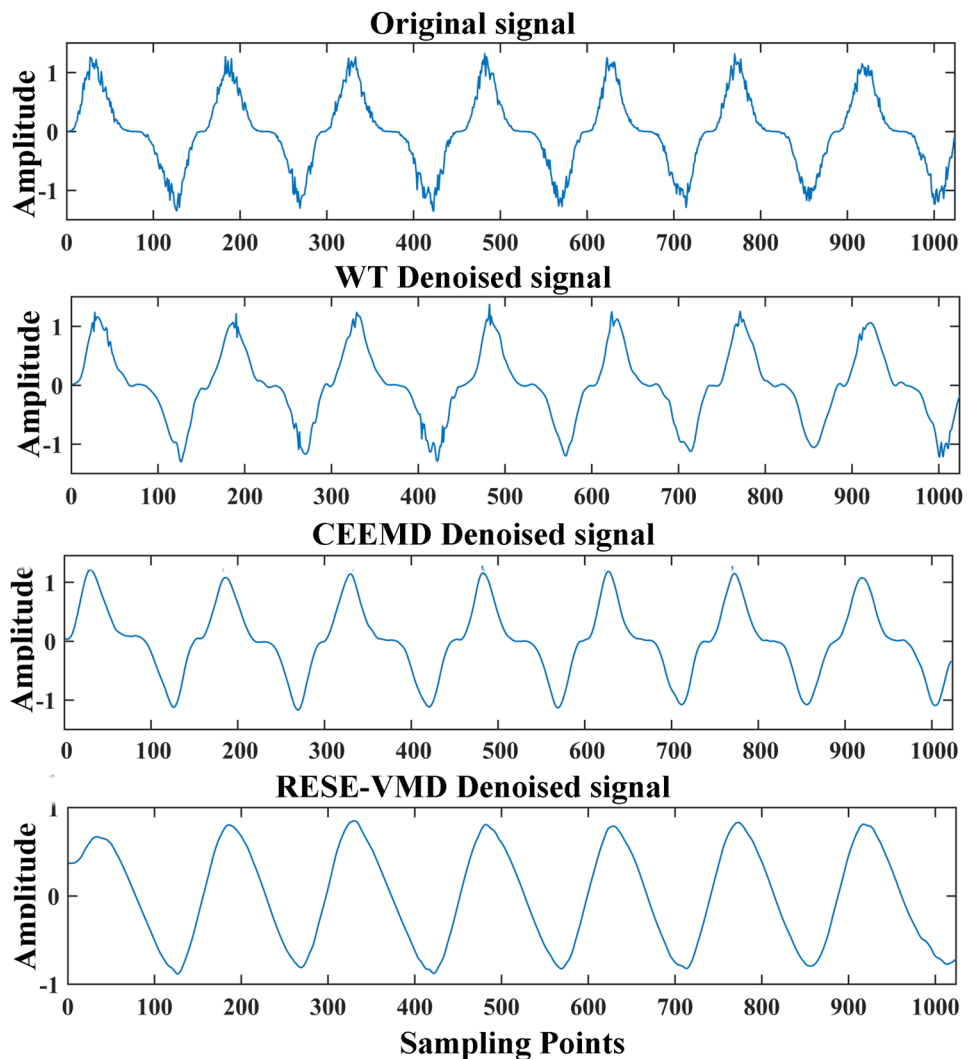
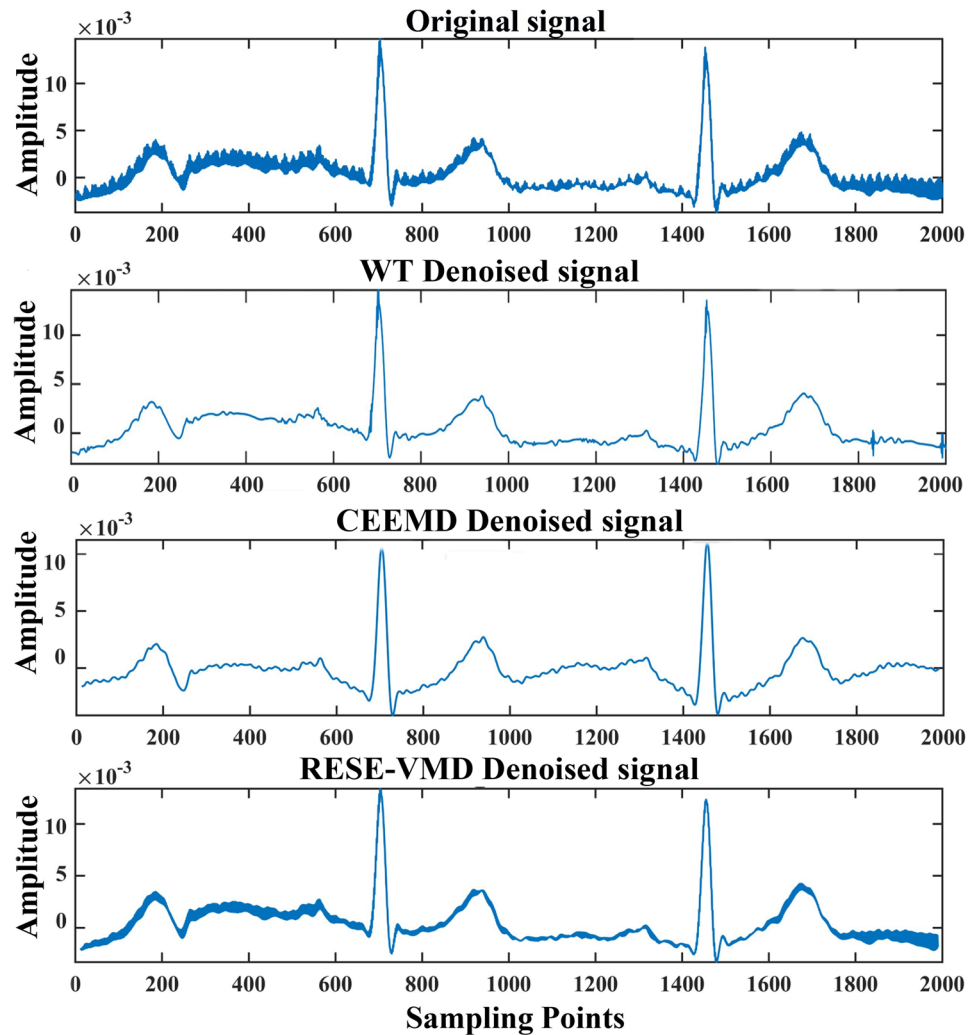


Figure 5 Denoising results of WT, CEEMD, and RESE-VMD on the heartbeat signal.



is used to optimize the parameters k and α are used to divide the signal into k modes. According to the sample entropy, the respiration and heartbeat signals are reconstructed to achieve denoising.

In order to verify the effectiveness of the algorithm, simulation experiments are carried out on the respiratory and heartbeat

signals. The respiratory signal simulation is carried out at an average respiratory rate of 20 breaths per minute, and the normal electrocardiogram data in the MIT-BIH database [31] are used as the heartbeat simulation data to avoid the influence of the respiratory harmonic noise error. The superiority of this method is verified by a comparison with other methods.

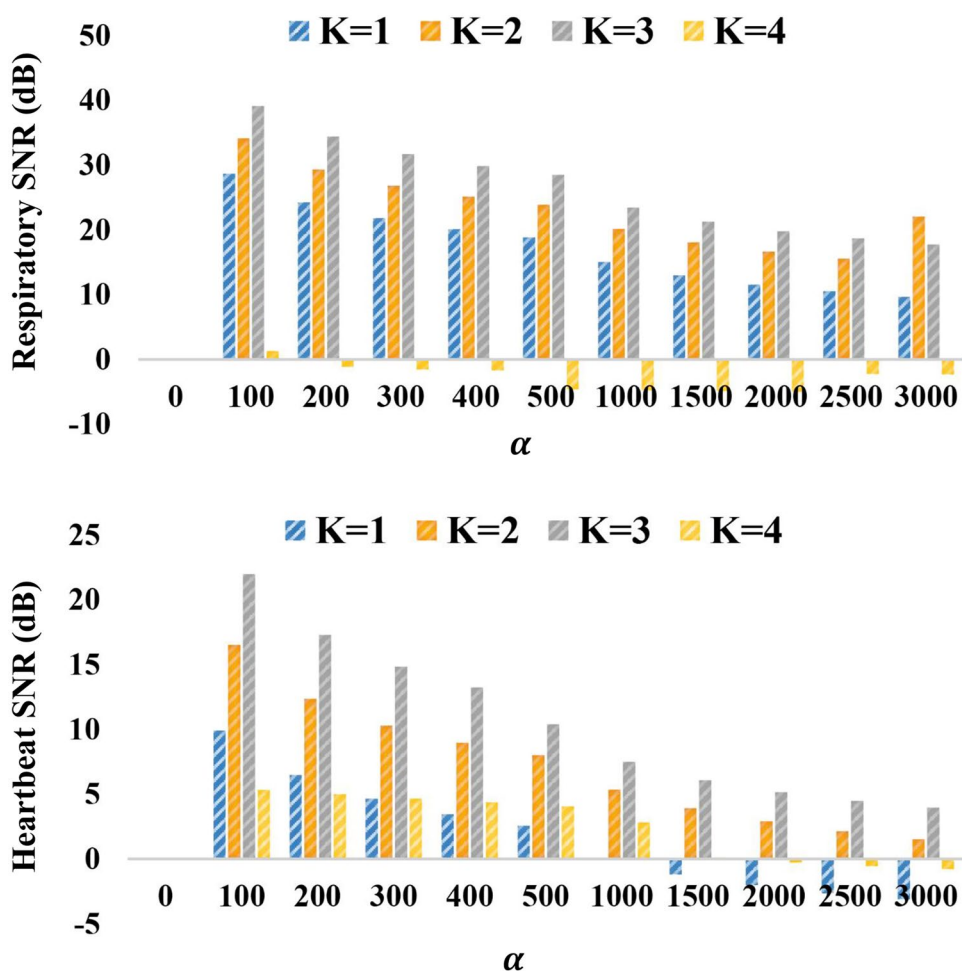
Table 2 Average SNR of respiratory signals at different Gaussian white noise.

Methods	SNR of respiration (dB)			
	5dB	10dB	15dB	20dB
WT	10.1635	12.3460	13.2571	15.1630
CEEMD	15.4690	16.4832	17.2511	18.3562
RESE-VMD	19.0226	21.3490	23.5574	25.5096

Table 3 Average SNR of heartbeat signals at different Gaussian white noise.

Methods	SNR of heartbeat (dB)			
	5dB	10dB	15dB	20dB
WT	9.1377	10.5691	11.7320	12.5411
CEEMD	10.7620	11.4821	12.0521	13.0982
RESE-VMD	17.8872	18.9381	19.1362	20.3110

Figure 6 SNR for parameters K and α .



Figures 4 and 5 show the denoising effects of WT, CEEMD, and RESE-VMD methods. The denoising waveform of the RESE-VMD method is smoother and retains

effective information. The denoising effect of the proposed method is the best.

Figure 7 RESE-VMD decomposition time-domain diagram and spectrogram of the respiratory signal.

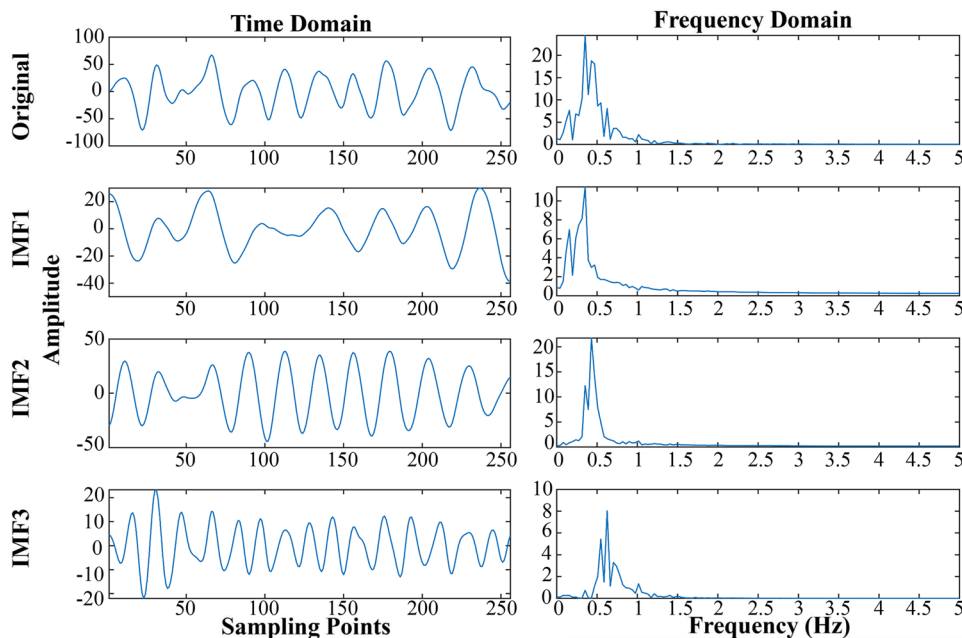
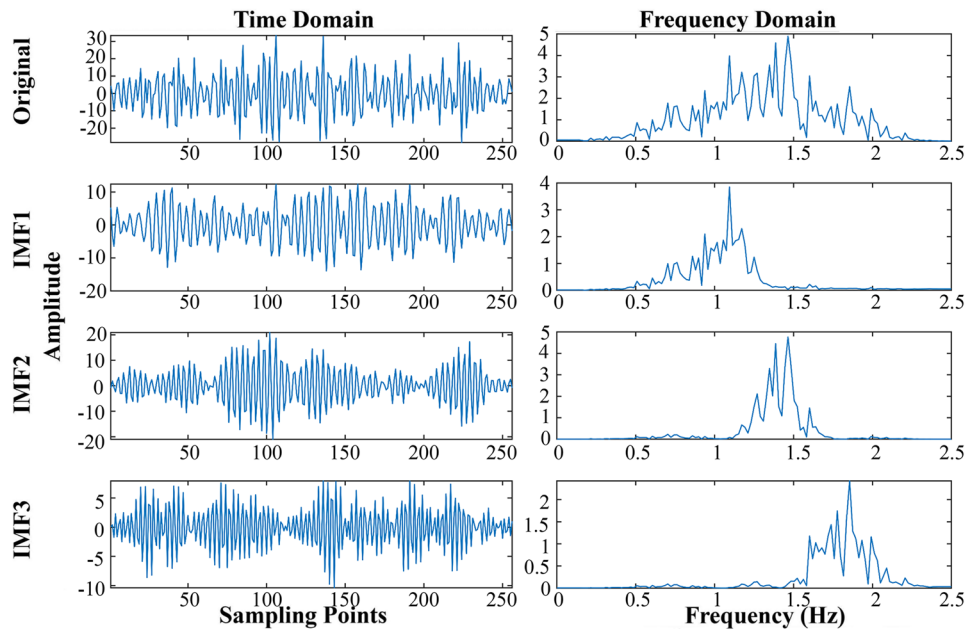


Figure 8 RESE-VMD decomposition time-domain diagram and spectrogram of the heartbeat signal.



In order to verify the accuracy as well as the reasonableness of the denoising effect, 200 experiments were carried out in this paper. Gaussian white noise of 5dB, 10dB, 15dB and 20dB were added to the original signal. As shown in Tables 2 and 3, we compare the average SNR values of 200 different experimental methods. The algorithm proposed in this paper achieves the highest SNR in the denoising process of the simulated signals. The denoising performance is better than other algorithms under different noise disturbances.

3.3 Optimize Parameters

k and α are automatically searched by the relative entropy method. To verify the effectiveness of the RESE-VMD

method, we carry out a manual parameter selection experiment on the real collected data. The respiratory signal's appropriate parameters are $k = 3$ and $\alpha = 100$, and the heartbeat signal's appropriate parameters are $k = 3$ and $\alpha = 100$. Figure 6 shows the results for various combinations of k and α . In Fig. 6, the maximum SNR for respiration is obtained when $k = 3$ and $\alpha = 100$. The maximum SNR for heartbeat is obtained when $k = 3$ and $\alpha = 100$. Therefore, our method can reduce the calculation time and improve work efficiency.

3.4 Extracting Vital Signs by RESE-VMD

Figures 7 and 8 show the time and frequency domain plots of respiration and the heartbeat by the RESE-VMD

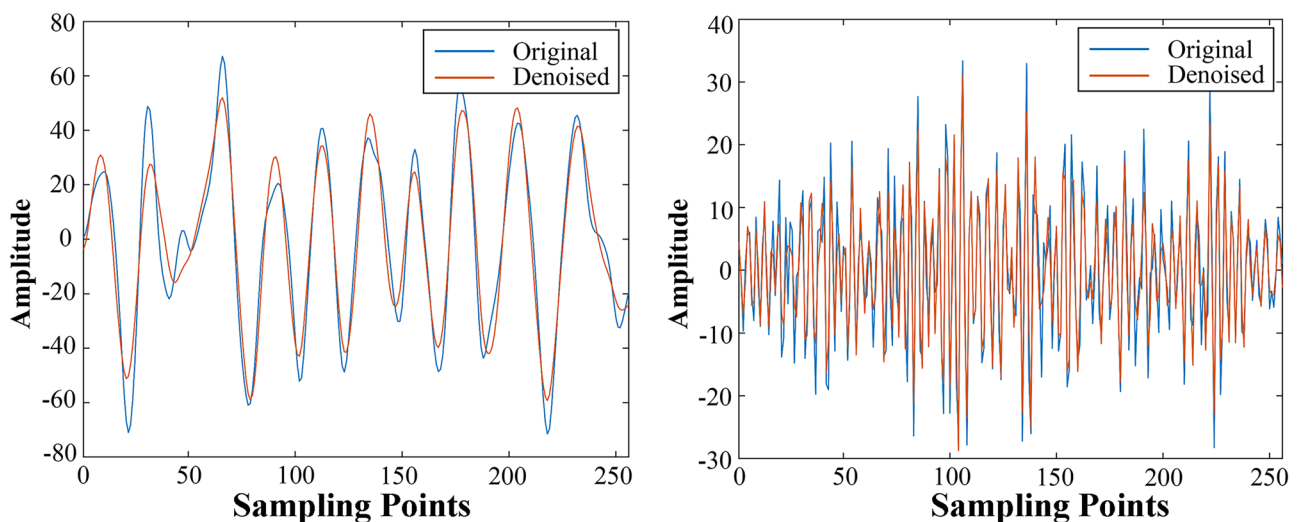


Figure 9 Respiration and heartbeat signals before and after RESE-VMD decomposition and reconstruction.

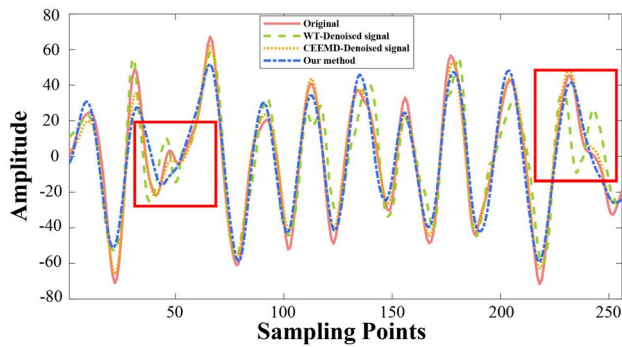


Figure 10 Comparison of the denoising effect of different methods for respiratory signals.

method, respectively. Respiration and the heartbeat are decomposed into three modal components. When the frequencies are within their respective frequency ranges, the sample entropy is applied to determine the vital sign signal content of each modal component. When the sample entropy is smaller, the signal content is higher and the noise content is lower. The appropriate modal component is selected according to the sample entropy for signal reconstruction and denoising.

Figure 9 shows respiration and heartbeat signals before and after reconstruction by the RESE-VMD method. Comparing the respiration and heartbeat signals before and after denoising, we can see that the significant denoising effect after applying the optimization algorithm, as well as the SNR, is greatly improved, which ensures that the effective signal is not lost during noise removal.

The vibration of the chest cavity caused by respiration is greater than that of the heartbeat. At the same time, the vibration is not easily affected by noise. To demonstrate the superiority of the presented algorithm, the WT, CEEMD, and RESE-VMD methods are used to denoise the real respiration signals. The red boxes in Fig. 10 show the error parts. Our method has a significant denoising effect on the error parts. The waveform after RESE-VMD denoising is smoother and has no false spectral peaks. The accuracy of subsequent calculations is guaranteed.

Table 4 SNR and runtime of respiration and heartbeat signals for different methods.

Methods	SNR of respiration (dB)	SNR of heartbeat (dB)	Times (s)
WT	13.2014	-6.6257	1.84
CEEMD	16.5067	11.7332	29.22
RESE-VMD	39.0974	21.9800	8.59

The bolded contents in the table indicate the results of the research method in this paper

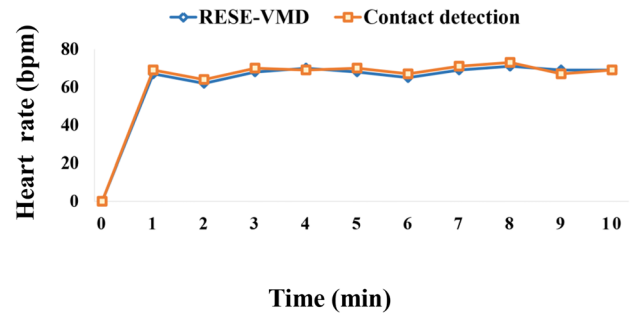


Figure 11 The results of the heartbeat detection by the RESE-VMD method and contact detection equipment in this paper.

Table 4 shows the SNR and times of the respiratory heartbeat signals under the three methods, and the SNR calculated by the optimized method achieves a significant enhancement. Due to the time-sensitive nature of vital signs. The program run time varies with the amount of data. Table 4 shows the running times for different methods for the same size of data. The WT method has the shortest running time but is less accurate, while the CEEMDAN method has the longest running time and is prone to untimely diagnosis. Therefore, the RESE-VMD method proposed in this paper is the best choice in terms of runtime and accuracy.

Figure 11 shows the results of the heartbeat detection by the RESE-VMD method and contact detection equipment in this paper. The experimental results show that the accuracy of noncontact heart rate detection reaches about 98%.

$$Ratio = \frac{R_{radar}}{R_{Reference}} \times 100\% \tag{23}$$

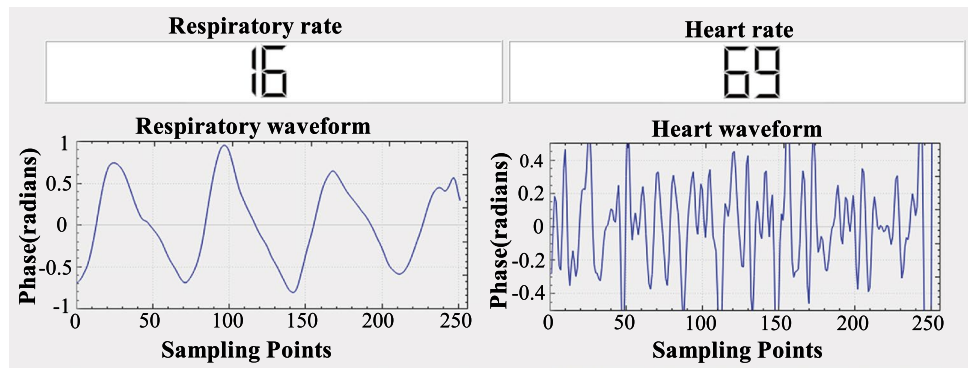
where R_{radar} is the result of the radar measurement, and $R_{Reference}$ is the result of the reference sensor.

3.5 System Interface Display

Figures 12 and 13 show the results of tester 1 and tester 2 while maintaining normal respiration. During the detection process, the system can smoothly display the waveform of respiration and heartbeat signals.

Figure 14 shows the test results, in which the tester 3 holds their breath; at the same time, the measured personnel respiratory rate is 0, and the respiratory waveform change is small and tends to zero. However, the heartbeat waveform is clear because the tester holds their breath. The displacement of the thoracic cavity is caused by the heartbeat. The displacement of the chest due to the human heartbeat is much smaller than that due to respiration. From normal respiration to apnea, thoracic displacement decreases gradually.

Figure 12 The first tester is about 0.6 m away from the radar. At this time, tester 1's respiratory rate is 16 breaths/minute, and their heartbeat rate is 69 beats/minute.



4 Discussion

The theoretical analysis, simulation, and experiment in the previous sections propose a new signal processing scheme to detect vital signs. Based on the experimental results, the accuracy of the method proposed in this paper can be considered reasonable.

The idea of detecting cardiopulmonary function using millimeter-wave radar technology realizes noncontact measurement. Its potential use is that in some applications, the monitoring equipment is not attached to the patient, which has the advantages of comfort and convenience. The signals obtained by the radar are the thoracic vibration signals caused by respiration and the heartbeat as well as the interference signals caused by the patient's involuntary movements. However, owing to the complexity of micromotion signal extraction and the error caused by human random motion, the idea has become an important research topic [32, 33]. This paper introduces a 77-GHz millimeter-wave radar device with a low cost and high sensitivity, which is used to detect vital signs and separate respiration and heartbeat signals. The system has achieved good results. However, errors such as patients' involuntary movement and power frequency noise generated by hardware are a key research direction in the future.

To reduce the influence of interfering signals, we propose the RESE-VMD method to separate respiratory and heartbeat signals. Range-FFT and MTI methods allow us to accurately determine the target and avoid the interference of static clutter. Phase unwrapping and phase differential are used to obtain phase information related to the heartbeat and respiration. The heartbeat and respiration signals are decomposed and reconstructed by the RESE-VMD method. The RESE-VMD method can reduce irregular waveforms, effectively reduce noise and harmonic interference, and retain the time-frequency characteristics of the original signal. Compared with the traditional band-pass filtering, WT and CEEMD, the RESE-VMD method separates the respiratory and heartbeat signals with higher accuracy.

In addition, when multiple millimeter-wave radars work close to each other at the same time, they interfere with each other. To avoid the influence of error, this paper only considers the measurement results of a single radar. After that, we further study the interaction between radars and how to reduce interference.

Although the potential of the proposed scheme is obvious, it still needs more research before clinical application. Owing to the above limitations of the proposed scheme, it is suggested that the application scenario be an environment with relatively stable objectives. In future work, we plan

Figure 13 The second tester is about 0.9 m away from the radar. At this time, tester 2's respiratory rate is 15 breaths/minute. The heartbeat rate is 74 beats/minute.

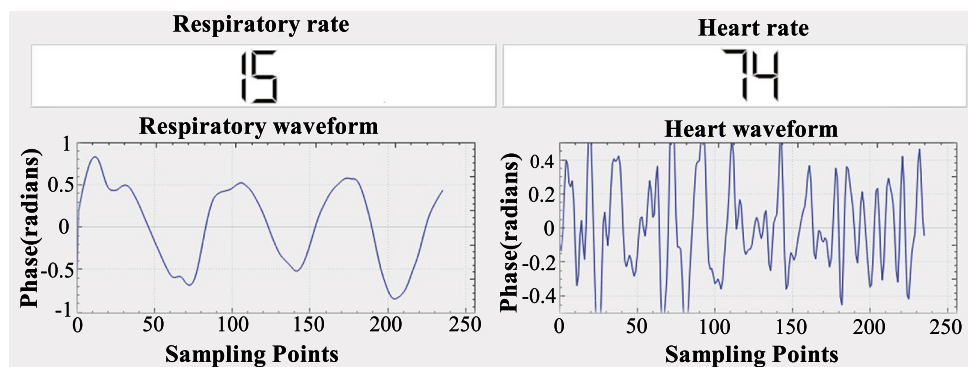
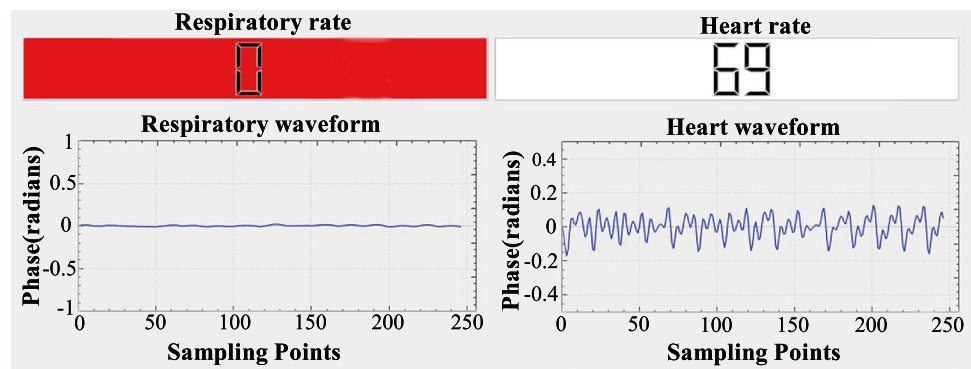


Figure 14 The third tester is about 0.9 m away from the radar. At this time, tester 3's respiratory rate is 0 breaths/minute. The heartbeat rate is 69 beats/minute.



to carry out further research and continuously improve the system to further improve its accuracy.

5 Conclusions

Noncontact vital sign detection is the current mainstream trend. This paper adopts the 77-GHz millimeter-wave radar signal acquisition system. We apply the relative entropy and sample entropy to optimize the VMD algorithm and introduce the RESE-VMD method into radar signal processing. The ideal parameters of the variational model are searched by relative entropy, and the signal is reconstructed by selecting the appropriate signal components according to the sample entropy. We propose the RESE-VMD method to realize the accurate separation of respiratory and heartbeat signals. Through simulation and real scene experiments, the denoising effect of the RESE-VMD method is found to be superior to other methods proposed in this paper, and the SNR ratio is greatly improved. The authenticity of the signal is preserved to a large extent, and more accurate results are obtained. The results of the heartbeat detection by our proposed method and contact detection equipment are given in this paper. The experimental results show that the accuracy of noncontact heart rate detection reaches about 98%.

Author Contributions K.W.: Methodology, Visualization, Writing - original draft; Y.Z. and J.G.: Supervision, Writing - review & editing.

Funding This research was funded by the National Natural Science Foundation of China (No. 62002208, No. 42271093), Natural Science Foundation of Shandong Province (No. ZR2019MA028, No. ZR2020MA082).

Declarations

Conflict of Interest The authors declare that the research was conducted in the absence of any commercial or financial relationships that could be construed as a potential conflict of interest.

References

1. Maurya, L., Kaur, P., Chawla, D., & Mahapatra, P. (2021). Non-contact breathing rate monitoring in newborns: A review. *Computers in Biology and Medicine*, *132*, 104321.
2. Elagan, S. K., Abdelwahab, S. F., Zanaty, E. A., Alkinani, M. H., Alotaibi, H., & Zanaty, M. E. (2021). Remote diagnostic and detection of coronavirus disease (COVID-19) system based on intelligent healthcare and internet of things. *Results in Physics*, *22*, 103910.
3. Guo, Y., Liu, X., Peng, S., Jiang, X., Xu, K., Chen, C., ... & Chen, W. (2021). A review of wearable and unobtrusive sensing technologies for chronic disease management. *Computers in Biology and Medicine*, *129*, 104163.
4. Johnson, J. E., Shay, O., Kim, C., & Liao, C. (2019). Wearable Millimeter-Wave device for contactless measurement of arterial pulses. *IEEE Transactions on Biomedical Circuits and Systems*, *13*(6), 1525–1534.
5. He, M., Nian, Y. J., & Gong, Y. S. (2017). Novel signal processing method for vital sign monitoring using FMCW radar. *Biomedical Signal Processing and Control*, *33*, 335–345.
6. Jeong, I. C., Bychkov, D., & Searson, P. C. (2019). Wearable devices for precision medicine and health state monitoring. *IEEE Transactions on Biomedical Engineering*, *66*(5), 1242–1258.
7. Alizadeh, M., Shaker, G., De Almeida, J. C. M., & Morita, P. P. (2019). Safavi-Naeini, remote monitoring of human vital signs using mm-wave FMCW radar. *IEEE Access*, *7*, 54958–54968.
8. Antolinos, E., García-Rial, F., Hernández, C., Montesano, D., Godino-Llorente, J. I., & Grajal, J. (2020). Cardiopulmonary activity monitoring using millimeter wave radars. *Remote Sensing*, *12*(14), 2265.
9. Kumar, A., Tomar, H., Mehla, V. K., Komaragiri, R., & Kumar, M. (2021). Stationary wavelet transform based ECG signal denoising method. *ISA Transactions*, *114*, 251–262.
10. Veerakumar, T., Subudhi, B. N., & Esakkirajan, S. (2019). Empirical mode decomposition and adaptive bilateral filter approach for impulse noise removal. *Expert Systems with Applications*, *121*, 18–27.
11. Satija, U., Ramkumar, B., & Manikandan, M. S. (2018). Automated ECG noise detection and classification system for unsupervised healthcare monitoring. *IEEE Journal of Biomedical and Health Informatics*, *22*(3), 722–732.
12. Rehman, N. U., & Aftab, H. (2019). Multivariate variational mode decomposition. *IEEE Transactions on Signal Processing*, *67*(23), 6039–6052.
13. Yang, X., Zhang, X., Ding, Y., & Zhang, L. (2021). Indoor activity and vital sign monitoring for moving people with multiple radar data fusion. *Remote Sensing*, *13*(18), 3791.

14. Kumar, S., Panigrahy, D., & Sahu, P. K. (2018). Denoising of Electrocardiogram (ECG) signal by using empirical mode decomposition (EMD) with non-local mean (NLM) technique. *Biocybernetics Biomedical Engineering*, 38(2), 297–312.
15. Cheng, Y., Wang, Z. W., Chen, B. Y., Zhang, W. H., & Huang, G. H. (2019). An improved complementary ensemble empirical mode decomposition with adaptive noise and its application to rolling element bearing fault diagnosis. *ISA Transactions*, 91, 218–234.
16. Zheng, P., Zheng, C., Li, X., Chen, H., Wang, A., & Luo, Y. (2022). Second harmonic weighted reconstruction for non-contact monitoring heart rate. *IEEE Sensors Journal*, 22(6), 5815–5823.
17. Chamaani, S., Akbarpour, A., Helbig, M., & Sachs, J. (2021). Matrix pencil method for vital sign detection from signals acquired by microwave sensors. *Sensors*, 21(17), 5735.
18. Li, Z., Jin, T., Dai, Y., & Song, Y. (2021). Through-wall multi-subject localization and vital signs monitoring using UWB MIMO imaging radar. *Remote Sensing*, 13(15), 2905.
19. Nazari, M., & Sakhaei, S. M. (2018). Variational mode extraction: A new efficient method to derive respiratory signals from ECG. *IEEE Journal of Biomedical and Health Informatics*, 22(4), 1059–1067.
20. Zhang, X., Liu, Z., Kong, Y., & Li, C. (2021). Mutual interference suppression using signal separation and adaptive mode decomposition in noncontact vital sign measurements. *IEEE Transactions on Instrumentation and Measurement*, 71, 1–15.
21. Prat, A., Blanch, S., Aguasca, A., Romeu, J., & Broquetas, A. (2019). Collimated beam FMCW radar for vital sign patient monitoring. *IEEE Transactions on Antennas and Propagation*, 67(8), 5073–5080.
22. Cao, Z. H., Li, J. J., Song, C. Y., Xu, Z. W., & Wang, X. P. (2021). Compressed sensing-based multitarget CFAR detection algorithm for FMCW radar. *IEEE Transactions on Geoscience and Remote Sensing*, 59(11), 9160–9172.
23. Zhang, X., Wang, F., & Li, H. (2022). An efficient method for cooperative multi-target localization in automotive radar. *IEEE Signal Processing Letters*, 29, 16–20.
24. Mercuri, M., Sacco, G., Hornung, R., Zhang, P., Visser, H. J., Hijdra, M., Liu, Y. H., Pisa, S., van Liempd, B., & Torfs, T. (2021). 2-D localization, angular separation and vital signs monitoring using a SISO FMCW radar for smart long-term health monitoring environments. *IEEE Internet of Things Journal*, 8(14), 11065–11077.
25. Zhang, X., Miao, Q., Zhang, H., & Wang, L. (2018). A parameter-adaptive VMD method based on grasshopper optimization algorithm to analyze vibration signals from rotating machinery. *Mechanical Systems and Signal Processing*, 108, 58–72.
26. Li, H., Chang, J., Xu, F., Liu, Z., Yang, Z., Zhang, L., ... & Liu, B. (2019). Efficient lidar signal denoising algorithm using variational mode decomposition combined with a whale optimization algorithm. *Remote Sensing*, 11(2), 126.
27. Wang, F., Zeng, X., Wu, C., Wang, B., & Liu, K. J. R. (2021). mmHRV: Contactless heart rate variability monitoring using millimeter-wave radio. *IEEE Internet of Things Journal*, 8(22), 16623–16636.
28. Kalpakis, K., Yang, S., Hu, P. F., Mackenzie, C. F., Stansbury, L. G., Stein, D. M., & Scalea, T. M. (2015). Permutation entropy analysis of vital signs data for outcome prediction of patients with severe traumatic brain injury. *Computers in Biology and Medicine*, 56, 167–174.
29. Wu, Q., & Lin, H. (2019). Daily urban air quality index forecasting based on variational mode decomposition, sample entropy and LSTM neural network. *Sustainable Cities and Society*, 50, 101657.
30. Porta, A., Bari, V., De Maria, B., Cairo, B., Vaini, E., Malacarne, M., Pagani, M., & Lucini, D. (2019). On the relevance of computing a local version of sample entropy in cardiovascular control analysis. *IEEE Transactions on Biomedical Engineering*, 66(3), 623–631.
31. Goldberger, A. L., Amaral, L. A. N., Glass, L., Hausdorff, J. M., Ivanov, P. C., Mark, R. G., Mietus, J. E., Moody, G. B., Peng, C. K., & Stanley, H. E. (2000). PhysioBank, PhysioToolkit, and PhysioNet - Components of a new research resource for complex physiologic signals. *Circulation*, 101(23), E215–E220.
32. Xiong, X., Deng, Z., Qi, W., Ou, H., & Cui, Z. (2019). A novel high-precision range estimation method based on phase of wide-band radar echo. *IEEE Transactions on Geoscience and Remote Sensing*, 57(6), 3392–3403.
33. Xiong, Y., Peng, Z., Gu, C., Li, S., Wang, D., & Zhang, W. (2020). Differential enhancement method for robust and accurate heart rate monitoring via microwave vital sign sensing. *IEEE Transactions on Instrumentation and Measurement*, 69(9), 7108–7118.

Publisher's Note Springer Nature remains neutral with regard to jurisdictional claims in published maps and institutional affiliations.

Springer Nature or its licensor (e.g. a society or other partner) holds exclusive rights to this article under a publishing agreement with the author(s) or other rightsholder(s); author self-archiving of the accepted manuscript version of this article is solely governed by the terms of such publishing agreement and applicable law.